



A long-term (2002 to 2017) record of closed-path and open-path eddy covariance CO₂ net ecosystem exchange fluxes from the Siberian Arctic

David Holl¹, Christian Wille², Torsten Sachs², Peter Schreiber³, Benjamin R.K. Runkle⁴, Lutz Beckebanze¹, Moritz Langer³, Julia Boike³, Eva-Maria Pfeiffer¹, Irina Fedorova⁵, Dimitry Yu. Bolshianov⁶, Mikhail N. Grigoriev⁷, and Lars Kutzbach¹

¹Institute of Soil Science, Center for Earth System Research and Sustainability (CEN), Universität Hamburg, Hamburg, Germany

²Helmholtz-Zentrum Potsdam – Deutsches GeoForschungsZentrum (GFZ), Potsdam, Germany

³Alfred Wegener Institute Helmholtz Centre for Polar and Marine Research, Potsdam, Germany

⁴Department of Biological & Agricultural Engineering, University of Arkansas, Fayetteville, USA

⁵Saint Petersburg State University – Institute of Earth Sciences, St. Petersburg, Russia

⁶Arctic and Antarctic Research Institute, St. Petersburg, Russia

⁷Permafrost Institute, Yakutsk, Russia

Correspondence: David Holl (david.holl@uni-hamburg.de)

Abstract. Ground-based observations of land–atmosphere fluxes are necessary to progressively improve global climate models. Observed data can be used for model evaluation and to develop or tune process models. In arctic permafrost regions, climate–carbon feedbacks are amplified. Therefore, increased efforts to better represent these regions in global climate models have been made in recent years. We present a multiannual time series of land–atmosphere carbon dioxide fluxes measured *in situ* with the eddy covariance technique in the Siberian Arctic (72° 22' N, 126° 30' E). The site is part of the international network of carbon dioxide flux observation stations (FLUXNET, Site ID: Ru-Sam). The dataset includes consistently processed fluxes based on concentration measurements of closed-path and open-path gas analyzers. With parallel records from both sensor types, we were able to apply a site-specific correction to open-path fluxes. This correction is necessary due to a deterioration of data, caused by heat generated by the electronics of open-path gas analyzers. Parameterizing this correction for subperiods of distinct sensor setups yielded good agreement between open and closed-path fluxes. We compiled a long-term (2002 to 2017) carbon dioxide flux time series that we additionally gap-filled with a standardized approach. The data set was uploaded to the Pangaea data base and can be accessed through <https://doi.pangaea.de/10.1594/PANGAEA.892751>.

Copyright statement. Authors 2018. This work is distributed under the Creative Commons Attribution 4.0 License.



1 Introduction

The release of the Arctic's belowground carbon (C) pools to the atmosphere can potentially act as a positive feedback on climate change. Organic material that is now stored in the permanently frozen soil and largely inaccessible for microbial decomposition might become available under a warming climate resulting in an increased release of greenhouse gases from Arctic regions (Schuur et al., 2015). At the same time, the Arctic vegetation responds to ongoing warming with a greening trend (Park et al., 2016), probably enhancing summer carbon assimilation. Although the importance of permafrost carbon pools for a potential amplification of climate change has been widely recognized (e.g. Zimov et al., 2006; Davidson and Janssens, 2006; Schuur et al., 2008; Khvorostyanov et al., 2008; Tarnocai et al., 2009; Koven et al., 2011; Schneider von Deimling et al., 2012; MacDougall et al., 2012; Schuur et al., 2013; McGuire et al., 2018), the earth system models analyzed for the Fifth Assessment Report (AR5) of the Intergovernmental Panel on Climate Change (IPCC) did not include permafrost carbon emissions.

While efforts to include permafrost dynamics into global climate models have been made recently (e. g. Wania et al., 2009a, b, 2010; Ekici et al., 2014; Kaiser et al., 2017; McGuire et al., 2018), models can be improved by using ground-based flux measurements for calibration and validation. McGuire et al. (2012) assessed the carbon balance of the Arctic tundra combining ground-based observations, process and atmospheric inversion models. The authors found that the uncertainty with which a carbon balance can be quantified is still very large, with upper and lower uncertainty bounds indicating the Arctic tundra as a sink for carbon at one and as a C-source at the other bound. McGuire et al. (2012) conclude that constraining inversion models relies on high quality ground-based measurements that should be placed strategically, e. g. along hydrological or vegetation gradients. *In situ* gas flux measurements from the Arctic are, however, still scarce. Moreover, the available data is biased towards Alaska, observations from the Eurasian Arctic are even more scarce (Oechel et al., 2014). To be able to distinguish climate change-related flux responses from interannual variability, long-term datasets are essential as recently argued by Baldocchi et al. (2017).

Within the scope of this publication, we aimed at creating a high quality, long-term CO₂ flux dataset from a polygonal tundra site in the Russian Arctic. We had the opportunity to analyze a 16 year record of eddy covariance data that includes periods with simultaneous measurements from two different (closed-path and open-path) CO₂ gas analyzer types. Our objective was to consistently process the data while following standardized quality control methods to allow for comparability between the different years of our record and with other datasets. We additionally aimed at cross-calibrating open-path and closed-path CO₂ fluxes and at gap-filling the dataset by employing the method of Reichstein et al. (2005) that is widely used in the FLUXNET community.

2 Site description

The investigation site is located on Samoylov Island in the southern central part of the Lena River Delta at 72° 22' N, 126° 30' E. The fan-shaped delta covers an area of roughly 30000 km² (Grigoriev, 1993; Schneider et al., 2009) and is characterized by a network of channels and more than 1500 islands (Antonov, 1967). Being the largest delta in the Arctic and one of the largest worldwide (Walker, 1998), it lies in the continuous permafrost zone with permafrost depths of about 500



to 600 m (Romanovskii et al., 2004; Yerшов, 2004; Brown et al., 1997). Mean annual permafrost temperatures range around -9 °C at 10 m depth (Romanovsky et al., 2010), making the Lena River Delta one of the coldest permafrost regions on earth. Boike et al. (2013) inferred an annual mean soil temperature of -8.6°C at 10.7 m depth from a 2006 to 2011 time series of temperature measurements in a borehole on Samoylov Island. Based on long-term hydrological observations in the delta area, Fedorova et al. (2015) found an increase in discharge as well as in sediment flux indicating recently intensified thawing of ice complex sediments in the region.

Grigoriev (1993) divides the delta area in three main geomorphological units. The oldest, ice-rich river terrace consists of fine-grained sediments with high organic content. It developed as an eroded Pleistocene plane characterized by polygonal ground and thermokarst processes. The second largest unit consists of Late Pleistocene to Early Holocene sandy sediments with low ice content and covers 23 % of the north-western part (Schneider et al., 2009). Samoylov Island is part of the third unit, the Mid to Late Holocene river terrace (Bolshiyarov et al., 2015), which makes up about two thirds of the delta (Schwamborn et al., 2002).

The island itself consists of two morphological units, an annually flooded, modern floodplain (1.49 km²) in the west and a Late Holocene river terrace (2.85 km²) in the east, which lies 10 to 16 m a.s.l. and is not flooded regularly (Kutzbach et al., 2007; Boike et al., 2013). The data presented here was collected with an eddy covariance system installed on the elevated river terrace. In contrast to the modern floodplain, the river terrace's surface is patterned due to frost-action that formed a wet polygonal tundra landscape consisting of low-centered ice-wedge polygons as well as thermokarst lakes and channels. Due to the underlying permafrost and thereby hampered drainage, water-saturated soils or ponds form in the polygon centers, whereas on the rims, which can be elevated up to 50 cm above the centers, a drier, moderately moist water regime prevails (Kutzbach et al., 2007; Helbig et al., 2013). Accordingly, the vegetation community in the wetter centers is dominated by hydrophytic sedges (*Carex aquatilis*, *Carex chordorrhiza*, *Carex rariflora*) and mosses (e. g. *Limprichtia revolvens*, *Meesia longiseta*, *Aulacomnium turgidum*). Mesophytic dwarf shrubs (e. g. *Dryas octopetala*, *Salix glauca*), forbs (e. g. *Astragalus frigidus*) and mosses (e.g. *Hylocomium splendens*, *Timmia austriaca*) dominate on the rims (Kutzbach et al., 2004; Pfeiffer and Grigoriev, 2002). Maximum summer leaf coverage was estimated by Kutzbach et al. (2004) to be 0.3 for vascular plants and 0.95 for mosses and lichens at both polygon centers and rims. The river terrace as a whole is composed of polygon rims with a coverage of 60 to 65 % and of depressed surfaces (including vegetated and water filled polygon centers as well as lakes and channels) that cover the remaining 35 to 40 % of area (Kutzbach et al., 2007; Sachs et al., 2010; Muster et al., 2012; Boike et al., 2013).

An arctic-continental climate with low mean annual temperatures prevails in the Lena River Delta. Although precipitation is low as well, the climate can be considered humid due to low evaporation rates (Kutzbach, 2006; Boike et al., 2008; Langer et al., 2011a, b). Based on long-term (1998 to 2017) *in situ* measurements on Samoylov Island, Boike et al. (2018) inferred an annual mean air temperature of -12.3 °C; the coldest and warmest months being February and July with mean temperatures of -32.7 °C and 9.5 °C respectively. For the period from 1998 to 2011, Boike et al. (2013) estimated total annual precipitation to be composed of 124 ± 57 mm summer rainfall and 65 ± 35 mm snowfall. Interannual variability in rainfall was, however, very high, with a maximum of 199 mm and a minimum of 48 mm. Snow melt usually starts in mid-May and lasts until early



June. Snow accumulation typically commences between late September and early October. Between 1998 and 2011, the snow season lasted on average 224 ± 18 days, the snow-free period 138 ± 18 days. Beginning in early to mid-June, the soil starts to thaw from the top, forming the so called active layer. Boike et al. (2013) report a mean active layer depth in August of 49 cm with a maximum of 79 cm between 1998 and 2011.

5 The soils of Samoylov Island were classified as *Gelisols* by Zubrzycki et al. (2013) based on work by Pfeiffer and Grigoriev (2002) according to the US Soil Taxonomy (Soil Survey Staff, 2014). On subgroup level, typical soils of the river terrace are *Glacic Aquiturbels*, which developed on the polygon rims and are characterized by the translocation of soil material due to freeze-thaw processes (cryoturbation). In the wetter polygon centers *Typic Historthels* formed. On the more sand-rich active floodplain, *Typic Aquorthels* and *Typic Psammorthels* dominate. According to the FAO World Reference Base for Soil
10 Ressources (IUSS Working Group WRB, 2015), the diverse soils of Samoylov Island belong to the reference soil group of *Cryosols*. Zubrzycki et al. (2013) estimated the soil organic carbon (SOC) stocks for the upper meter of the island's two major landscape units to be $29 \pm 10 \text{ kg m}^{-2}$ for the river terrace and $14 \pm 7 \text{ kg m}^{-2}$ for the active floodplain.

Since the scientific investigation of Samoylov Island commenced, gas exchange between the soils of the island and the atmosphere has been a research focus. While results on methane exchange fluxes and the soils' methane production and
15 oxidation potential are more prominent in the publication record (e.g. Wagner et al., 2003; Kutzbach et al., 2004; Liebner and Wagner, 2007; Knoblauch et al., 2008; Sachs et al., 2008; Wille et al., 2008; Schneider et al., 2009; Sachs et al., 2010; Liebner et al., 2011; Knoblauch et al., 2015, 2018), literature on CO_2 flux time series recorded with the same measurement system presented in this publication is available as well (Kutzbach, 2006; Kutzbach et al., 2007; Runkle et al., 2013; Zona et al.,
20 in review). The micrometeorological station on Samoylov Island is part of the international network of EC carbon dioxide flux observation sites (FLUXNET, Site ID: Ru-Sam). Kutzbach et al. (2015) contributed EC flux data from this measurement system to the FLUXNET2015 dataset.

3 Methods

3.1 Instrumentation

We used the eddy covariance (EC) technique to determine half-hourly gas and energy fluxes. The EC method requires high
25 frequency (typically $> 10 \text{ Hz}$) raw gas concentration and three-dimensional wind speed measurements. A comprehensive description of the EC approach is given for example by Aubinet et al. (2012). We recorded carbon dioxide (CO_2) and water vapor concentrations as well as three-dimensional wind speed with changing instrumentation on three different tower structures, all located on the central river terrace of Samoylov Island between 2002 and 2017 (see Fig. 1). We deployed open-path (OP) as well as closed-path (CP) gas analyzers, at times simultaneously. Models, manufacturers and years of deployment are given in
30 Table 1. Between the different setups, CP intake tube lengths varied from 5 to 8 m. OP analyzers were always installed inclined by about 10 degrees from the vertical, as suggested in the analyzer manuals. Raw data was recorded at 20 Hz except for the periods 22 August 2009 to 19 July 2010 (10 Hz) and 31 August 2012 to 17 May 2013 (5 Hz). Until 29 April 2014, all raw data were recorded on a CR3000 data logger (Campbell Scientific, UK). From then on, CP analyzer and anemometer data were

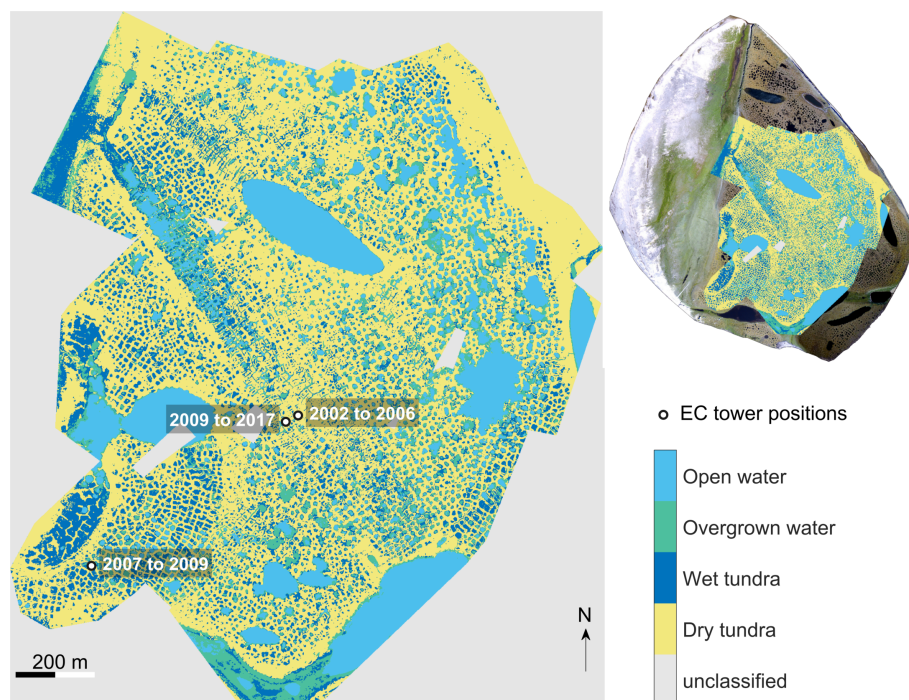


Figure 1. Eddy covariance (EC) tower positions on the river terrace of Samoylov Island and surface class distribution according to Muster et al. (2012). Photographic image of the entire island (top right corner) from Boike et al. (2012).

logged on a CR3000 whereas OP analyzer and anemometer data were recorded on a LI-7550 data logger (Licor Biosciences, USA). Although data coverage is biased towards the growing season, the data set contains year-round fluxes in some years (see Table 1).

3.2 Flux processing

5 3.2.1 Prior considerations

Due to the contrasting designs of OP and CP analyzers, these sensor types have distinct signal response characteristics that we considered during data processing. The most apparent constructional difference between OP and CP gas analyzers is the presence or absence of a housing for the measurement cell that contains the optical path. In a CP instrument, the measurement cell is housed whereas the optical path of an OP analyzer is exposed to the atmosphere. CP systems are typically more bulky and installed at the base of an EC tower, from where tubing leads to an intake close to the anemometer. Sample air is drawn into the cell with a pump. OP sensors are commonly installed in close proximity to the anemometer and do not require a pump. Due to the tubing acting as a low-pass filter, the response to high-frequency concentration variations is systematically attenuated in CP setups, as opposed to OP systems (Ibrom et al., 2007a). Moreover, the severity of frequency dampening can vary non-linearly with environmental conditions, especially with relative humidity (Runkle et al., 2012). CP analyzers have the



advantage of controlled temperature and pressure conditions in the measurement cell, allowing for the calculation of mixing ratios rather than molar densities (Ibrom et al., 2007b) and thereby avoiding the need to apply air density fluctuation correction terms.

These Webb-Pearman-Leuning (WPL, Webb et al., 1980) terms have to be included when using OP data to calculate EC
5 fluxes, as the optical path is exposed to the varying temperature and humidity conditions of the atmosphere. Additional sources of uncertainty are introduced when applying WPL terms, as their quality relies on not only precise but accurate concentration measurements as well as on undisturbed heat fluxes. Especially at times of low gas fluxes, WPL terms can become orders of magnitude larger than raw gas fluxes (Munger et al., 2012). Major drawbacks of OP instruments, especially in harsh environments, are (1) their downtime during adverse weather conditions (e. g. precipitation) and (2) flux biases due to sensor
10 self-heating (Burba et al., 2006, 2008). The OP self-heating effect was first recognized (Burba et al., 2006) due to apparent off-season CO₂ uptake in flux time series obtained with LI-7500 (LI-COR Biosciences, USA) OP gas analyzers. However, Kittler et al. (2017) recently found that this effect is not limited to cold conditions but extends throughout all seasons. The necessary corrections can be substantial but decrease largely when the sensor is not mounted vertically but inclined instead as shown by Rogiers et al. (2008) and Järvi et al. (2009).

15 3.2.2 Processing steps

We performed separate flux processing steps on OP and CP data sets and computed half-hourly fluxes using the software EddyPro (Licor Biosciences, USA). An overview of the processing steps is given in Table 2. We detected and removed raw data spikes according to Vickers and Mahrt (1997), with a maximum of 1 % accepted spikes and a maximum of three samples as consecutive outliers. We applied an angle of attack correction, i.e. compensation for flow distortion induced by the anemometer
20 frame (Nakai et al., 2006), on wind speed data collected with the R3 (Gill Instruments Ltd., UK) anemometer. The majority of the wind speed records come, however, from a CSAT3 (Campbell Scientific, UK) instrument for which this correction is not necessary. Coordinate rotation to align the anemometer x-axis to the current mean streamlines was calculated as double rotation according to Kaimal and Finnigan (1994). For OP fluxes, we compensated for air density fluctuations due to thermal expansion/contraction and water dilution/concentration following Webb et al. (1980). Because simultaneous water vapor concentration, cell temperature and cell pressure measurements from inside the CP analyzer were available, CO₂ concentrations
25 from this sensor could be converted directly into mixing ratios, i.e. concentrations referring to dry air of constant temperature (Ibrom et al., 2007b; Burba et al., 2012), making further corrections for density fluctuations unnecessary. We compensated CP time lags by using the automatic timelag optimization option in EddyPro. For this procedure, prior to processing the complete dataset, time lags were determined for a subperiod of raw data by covariance maximization (Fan et al., 1990). A searching window around the median of the found time lags (nominal timelag, T_{nom}) is defined by $T_{nom} \pm 3.5 \times MAD$, where MAD is
30 the median absolute deviation of the found time lags. When processing the complete dataset, EddyPro performed a covariance maximization of vertical wind speed and the scalar of interest for each half hour and then checked, whether the found time lag fell within the searching window defined before. If not, T_{nom} was used as time lag. Water vapor concentration time series were binned in ten RH-classes, and the procedure was applied to each class, resulting in ten different nominal time lags. CO₂



concentrations were not binned in humidity-classes. We computed CP time lag statistics annually and within a year if pump speeds or instrumental setups varied. OP time lags were determined by covariance maximization within a searching window of -10 to 10 seconds. We evaluated OP time lags statistics, binned in classes of wind direction sectors, later on in the course of quality filtering.

5 Spectral attenuation in the high- and the low-frequency spectral range was compensated according to the following methods. Low-frequency signal loss due to the finite averaging time used for flux calculations (30 minutes) and due to linear raw data detrending was corrected for following the method of Moncrieff et al. (2004) for both OP and CP fluxes. High-frequency signal loss of OP fluxes due to path and volume averaging of the sonic anemometer and the gas analyzers as well as due to the separation between the two instruments were corrected for with the analytical approach of Moncrieff et al. (1997). High-frequency
10 signal loss of CP fluxes due to spectral attenuation by the intake tube and volume averaging in the measurement cell were corrected for using the *in situ* method of Ibrom et al. (2007a). For each measurement period with a unique instrumental setup and CP pump speed, we determined the cut-off frequency of a first-order low-pass filter from ensemble means of 30-minute power spectra of CO₂ concentration and sonic temperature time series data. The spectral correction factor was then parametrized as a function of the cut-off frequency found and the mean wind speed for stable and unstable atmospheric conditions as described
15 by Ibrom et al. (2007a). Before using them for ensemble spectra estimations, the 30-minute power spectra were quality-filtered by applying the scheme of Vickers and Mahrt (1997), and by omitting half-hours that were assigned quality class 2 according to Mauder and Foken (2004). High frequency noise was removed from the ensemble means of CO₂ concentration power spectra before the determination of the cut-off frequency where it was deemed necessary. High-frequency signal losses due to crosswind and vertical separation of the sample air tube intake and the anemometer were corrected for according to Horst and
20 Lenschow (2009). Additionally, we set EddyPro to calculate random flux uncertainty estimates (Finkelstein and Sims, 2001) and three quality flags, which represent flux quality in values from 0 to 2 with 0 denoting the highest quality class as proposed by Mauder and Foken (2004). This quality evaluation is based on tests for stationarity and developed turbulence and thereby indicates whether general EC assumptions about atmospheric conditions were met during a flux calculation period.

3.3 Quality filtering

25 Flux quality assessment was largely based on the scheme of Mauder and Foken (2004), representing flux quality in three classes (0, 1 and 2). We applied additional screening steps and flagged fluxes of low quality. If a flagged flux was not already assigned to class 2 according to Mauder and Foken (2004), we set the quality flag to 2. We performed six additional flagging steps in the following sequence.

In **step 1**, skewness and kurtosis were computed with EddyPro for the half-hourly high frequency raw data time series of
30 CO₂ concentration, vertical wind speed and sonic temperature. If any of these statistics was outside certain intervals (skewness: $[-2, 2]$, kurtosis: $[1, 8]$, equivalent to the hard flag defined by Vickers and Mahrt (1997)), CO₂ flux values were flagged.

In **step 2**, OP fluxes were additionally filtered for an instrument signal strength indication (*AGC*) recorded from the LI-7500 sensor. Along with a software upgrade, this diagnostic value was renamed to *RSSI*, and its definition was changed. We therefore recalculated the *AGC* values for sensors not running on firmware version 6.6 and above (before July 2013). According to



the old *AGC* definition in the LI-7500 manual, typical clean window values range between 55 to 65 %. As dirt accumulates on the windows (or anywhere in the optical path), the *AGC* value will increase up to 100 %. The new *RSSI* value takes 100 % for clean windows and decreases as windows get dirtier. In order to obtain one consistent diagnostic variable for the cleanliness of the optical path, *AGC* was converted to the *RSSI* range. *AGC* values smaller than 44 were set to 44, then *AGC* values were mapped to the *RSSI* range as follows.

$$RSSI(AGC) = 188 - 2 \cdot AGC \quad (1)$$

We flagged OP CO₂ flux values when $RSSI \leq 60$.

As quality control of the half-hourly time lag detection results was not applied during OP flux processing in EddyPro, we additionally screened OP time lags to identify low quality flux values in **step 3**. We divided the time lag data set into subsets of different instrumental setup, and binned the time lags of these subsets in 36 ten degree wind direction sectors. We used the 25th and 75th percentiles per class as filter thresholds. We flagged OP flux values with associated time lags outside the range spanned by these thresholds. Because we computed CP fluxes in EddyPro considering and compensating for low time lag detection quality, we did not perform this type of filtering step on CP fluxes.

In **step 4**, we flagged CP as well as OP fluxes when 30 minute average concentration measurements were larger than 450 ppm or smaller than 300 ppm. CO₂ concentrations outside this range indicate dirty OP gas analyzer optics or technical problems of the CP air sampling system (sudden pump speed changes due to brownouts, blocked filters, etc.).

To filter dubious, large OP fluxes that coincided with reasonable CP fluxes, we selected all OP fluxes when simultaneously measured CP values ranged between $-2 \mu\text{mol m}^{-2} \text{s}^{-1}$ and $2 \mu\text{mol m}^{-2} \text{s}^{-1}$. **Step 5** only affected OP data from this subset. We calculated the 99th and 1st percentile of this group and flagged fluxes from it when they lay outside this percentile range.

In **step 6**, we flagged remaining outliers in both the CP and OP data sets by using the 0.1st and 99.9th percentile ($-3.5423 \mu\text{mol m}^{-2} \text{s}^{-1}$ and $3.3473 \mu\text{mol m}^{-2} \text{s}^{-1}$) of the CP time series after the concentration limits filter as absolute limits, to define an acceptable range of OP and CP flux values. In the dataset available for download, we included one column for each analyzer type containing a quality flag that can take values from 0 to 2 based on the scheme of Mauder and Foken (2004). As described above, we additionally assigned fluxes that did not meet our quality criteria to quality class 2. In our opinion, fluxes of quality class 2 should be omitted from further analysis. They are included in the reported dataset for the sake of completeness.

3.4 Open-path self-heating correction

To account for self-heating errors induced by the LI-7500 sensor electronics, we corrected OP fluxes as described by Kittler et al. (2017). The authors use WPL-corrected fluxes and add a correction term (Burba et al., 2006) that accounts for self-heating effects of vertically installed instruments. In their approach, Kittler et al. (2017) use a scaling factor ξ , taking values between 0 and 1, to trim the correction for inclined analyzer setups. With simultaneously available CP fluxes, we were able to estimate this scaling factor specifically for our site and periods of unique instrumental setups. As suggested by Kittler et al. (2017), we optimized this parameter with a nonlinear least squares method in Matlab (v. 9.2). We determined ξ for periods of different instrumental setups and separately for night (incoming shortwave radiation $< 20 \text{ Wm}^{-2}$) and day (incoming

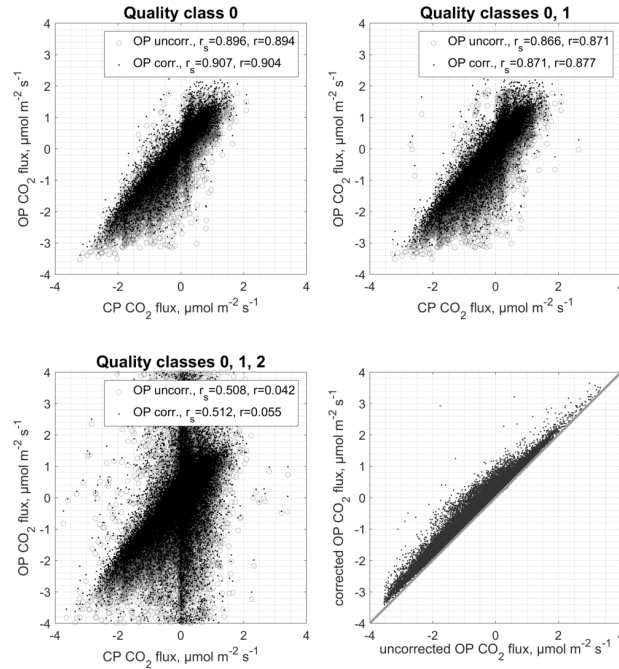


Figure 2. Fluxes from closed-path (CP) versus open-path (OP) analyzers. The agreement between CP and OP fluxes increases throughout all quality classes after OP correction. Correlations were quantified using Spearman’s rank correlation coefficient r_s and Pearson’s correlation coefficient r . The right panel in the bottom row shows the effect of the applied self-heating correction on OP fluxes.

shortwave radiation $\geq 20 \text{ Wm}^{-2}$) conditions using the following equation

$$F_c = F_{c,WPL} + \xi \frac{(T_s - T_a)\rho_c}{r_a T_a} \quad (2)$$

where F_c ($\text{kg m}^{-2} \text{ s}^{-1}$) is the true CO_2 flux, $F_{c,WPL}$ ($\text{kg m}^{-2} \text{ s}^{-1}$) is the WPL-corrected OP CO_2 flux, T_s (K) is the instrument surface temperature, T_a (K) the ambient air temperature, r_a (sm^{-1}) the aerodynamic resistance and ρ_c (kg m^{-3}) the ambient CO_2 density. Prior to ξ optimization, we estimated the instrument surface temperature T_s following the parameterization of Järvi et al. (2009) also separately for nighttime and daytime

$$T_{s,day} = 0.93(T_a - T_0) + 3.17 + T_0 \quad \text{and} \quad T_{s,night} = 1.05(T_a - T_0) + 1.52 + T_0 \quad (3)$$

with $T_{s,day}$ (K) and $T_{s,night}$ (K) as instrument surface temperature estimates and T_0 set to 273.15 K. We determined the scaling factor as a parameter of equation (2) being the modified Burba et al. (2006) approach from Kittler et al. (2017). For function fitting, we assumed CP fluxes of quality classes 0 and 1 as true fluxes. We used WPL-corrected OP quality class 0 fluxes and the above described surface temperature estimates as independent variables. Before parameter optimization, we quality-screened the Burba et al. (2006) correction term (expression to the right hand side of ξ in equation (2)) and removed spikes ranging within the uppermost or lowest percent of its distribution. Throughout all years, ξ is larger at daytime than at



nighttime but generally small, adding mostly below 1 % of the full correction term to the uncorrected flux (see Table 4). In four of the seven available years with simultaneous CP and OP fluxes, nighttime ξ optimization converged to values below zero. Before applying the correction models to these periods, we set nighttime ξ estimates to the median of the years yielding parameter values that, including their 95 % confidence bounds, ranged above zero. We used this value and the median of all daytime model optimizations to calculate corrected OP fluxes at times without parallel CP measurements. We did not correct OP fluxes when radiation measurements or correction term estimates were not available. Correlation between CP and OP fluxes improved throughout all quality classes by applying the self-heating correction, while fluxes indicating net CO₂ uptake were affected more strongly than fluxes above zero (see Fig. 2).

3.5 Carbon dioxide flux gap filling

We used the CP and the corrected OP fluxes (see Fig. 3) to compile a CO₂ flux time series. We aimed at keeping as many measured data points as possible, while omitting records with large uncertainty. We accepted all CP values of quality classes 0 and 1. At time steps where no CP fluxes were available, we selected OP values of the same quality classes. The resulting time series contains 75,921 datapoints. Additionally, we filled the remaining gaps in the time series using the marginal distribution sampling (MDS) method as first presented by Reichstein et al. (2005). This method employs two types of model value calculations. The environmental variables global radiation, air temperature and water vapour pressure deficit are binned in classes and combined in a look-up table (LUT). In case of a gap, flux values related to similar environmental conditions can be looked up and used for averaging and gap filling. The setup of different LUTs for fixed time periods has been first described by Falge et al. (2001). This process can be refined by the use of moving time windows (Moffat et al., 2007) around gaps, as applied by Reichstein et al. (2005). The second model type implemented in the MDS algorithm exploits the commonly high autocorrelation of gas flux time series. The mean diurnal variation (MDV) technique has as well been first described by Falge et al. (2001) and uses the average of available gas flux measurements from adjacent days at the same hour of day to fill a flux gap. The MDS method found wide application, as it has for example been the standard technique within the processing pipeline of the FLUXNET2015 data set, which includes over 1500 site-years of data. The algorithm of Reichstein et al. (2005) combines a screening procedure of the available data for similar environmental conditions (look-up table steps) and the use of a MDV method (diurnal cycle steps) if a gap could not be filled within the look-up table steps. Both techniques include moving windows with variable sizes that are increased until a solution can be found. Large gaps are skipped. To run the gap filling algorithm, we used the REddyProc routine that is accessible through a web-based service hosted by the Department of Biogeochemical Integration at Max Planck Institute Jena. The R-routine that is executed on this server is a further-developed and extended version of the Reichstein et al. (2005) approach and is described by Wutzler et al. (2017). We did not use the friction velocity filter or the flux partitioning capabilities of the REddy Proc online tool. Gap filling resulted in 131,908 datapoints. The provided data set includes quality flags for each gap-filled value that depend on the used method and time window size, as defined by Reichstein et al. (2005). These flags take values between 0 and 3, with 0 denoting measurement data, 1 indicating most reliable and 3 least reliable gap-filled fluxes. To assess the overall quality of the gap filling result, the MDS algorithm, in a stepwise manner, treats single available values as gaps and fills them according to the described scheme. Pearson's correlation



coefficient between our compiled CO₂ flux time series and the MDS quality assessment run, where these values were treated as artificial gaps, is 0.92, with a root mean squared error of 0.31 $\mu\text{mol m}^{-2} \text{s}^{-1}$.

3.6 Footprint modeling

In order to quantify the cumulative contribution of distinct surface classes to the EC source area, we evaluated the two-dimensional analytical footprint formulation described by Kormann and Meixner (2001) in combination with a 0.14 m × 0.14 m resolution surface classification of Samoylov Island's central river terrace provided by Muster et al. (2012). The authors divide the surface into four classes based on hydrology and vegetation communities, as illustrated in Fig. 1. Kormann and Meixner (2001) presented an analytical solution to the crosswind-distributed advection-diffusion equation described by Van Ulden (1978) and Horst and Weil (1992). Using the analytical model of Huang (1979), the authors solved the power-law profiles of horizontal wind velocity and eddy diffusivity by relating them to the Monin-Obukhov similarity theory, including the stability dependence of the exponents in the power laws at a certain height. We implemented the equations given in Kormann and Meixner (2001) as a Matlab (v. 9.2) function and added a quality filter, omitting calculations when friction velocity was larger than 0.9 m s^{-1} or smaller than 0 m s^{-1} , wind speed was below zero or above 20 m s^{-1} , the crosswind standard deviation was below zero or above 3 m s^{-1} or Monin-Obukhov length was smaller than 10⁻³ m or larger than 10⁴ m. Prior to half-hourly footprint calculations, we additionally determined roughness length statistics for annual subsets of data and binned them in 2° wind direction classes. The medians of these classes were used in the subsequent half-hourly footprint estimation, depending on the mean wind direction during these 30 minutes.

4 Data availability

The data set was uploaded to the Pangaea data base (Holl and Kutzbach, 2018) and can be accessed through <https://doi.pangaea.de/10.1594/PANGAEA.892751>. The included columns are given in Table 6.

5 Conclusions

We are confident that the presented carbon dioxide land-atmosphere flux data set is of high quality and is likely to be of value to the scientific community. We screened the data carefully and applied filtering rules to identify erroneous data, taking into account sensor diagnostics, time lag statistics and the presence of atmospheric conditions that allow for a robust application of the EC method. We followed standardized processing and quality control/assurance routines to allow for comparability between different years from our site as well as with flux time series from other tundra environments. With OP measurements being paralleled by CP measurements in seven years, we had the opportunity to correct for self-heating errors in our OP measurements with a site-specifically scaled correction term, rather than using default correction methods (e. g. Burba et al., 2008). We could therefore address different sensor setups with different correction terms and thereby improve our OP data set, as the self-heating effect has distinct impacts on sensors installed at different inclinations. We quantified the contribution of



certain soil and vegetation community types to each half-hourly EC footprint, taking into account varying roughness lengths throughout different years and wind direction sectors. We estimated the cumulative probability of being the EC source area for the four main surface classes on Samoylov Islands' river terrace by using a classified image and by computing an analytical footprint model. Multiannual results show (see Table 5) that on average the combination of different surface classes within the EC footprint is representative for the surface composition of the whole river terrace that developed as a polygonal tundra landscape. According to Muster et al. (2012) the river terrace is composed of 65 % *dry tundra*, 19 % *wet tundra* and 16 % ponds (sum of *open water* and *overgrown*). On average, the surface class compositions within the EC footprint are very similar to these values. Deviations arise, however, in the years between 2007 and 2009, when the tower location was shifted from the center towards the south-western cliff of Samoylov Island. Nevertheless, the contributions of each surface class to the EC footprint are not only available on average, as presented in Table 5, but half-hourly in the uploaded data set, ensuring that EC source area deviations are quantifiable by a potential user. 16 years of consistently processed and quality-controlled carbon dioxide fluxes from a polygonal tundra landscape typical for Arctic lowlands are a valuable addition to the already existing data base of CO₂ net ecosystem exchange observations from the Arctic, especially because of the site's location in Northern Siberia, from where only limited data is available up to now.

15 *Competing interests.* No competing interests are present.

Acknowledgements. Without the dedicated work of many scientists, logistics experts and engineers over the years, we would not have been able to present this long-term eddy covariance NEE data set. We want to thank Niko Bornemann, Tim Eckhardt, Mauel Helbig, Lars Heling, Oliver Kaufmann, Zoé Rehder, Norman Röbger, Norman Rüggen, Günter Stoof and Waldemar Schneider for their commitment, diligence and ingenuity. We thank Jakob Sievers for providing us with a starting point for the Matlab implementation of the Kormann and Meixner (2001) footprint model. This work was supported through the Cluster of Excellence CliSAP (EXC177), Universität Hamburg, funded through the German Science Foundation (DFG), by the European Commission through the project PAGE21 (FP7-ENV-2011, 282700) and by the German Ministry of Education and Research (BMBF) through the projects CarboPerm (03G0836A) and KoPf (03F0764A).



References

- Antonov, V.: The Lena river delta, Hydrometeoizdat, Leningrad, USSR, 1967.
- Aubinet, M., Vesala, T., and Papale, D.: Eddy covariance: a practical guide to measurement and data analysis, Springer, 2012.
- Baldocchi, D., Chu, H., and Reichstein, M.: Inter-annual variability of net and gross ecosystem carbon fluxes: A review, *Agricultural and Forest Meteorology*, 2017.
- Boike, J., Wille, C., and Abnizova, A.: Climatology and summer energy and water balance of polygonal tundra in the Lena River Delta, Siberia, *Journal of Geophysical Research: Biogeosciences*, 113, 1–15, 2008.
- Boike, J., Grüber, M., Langer, M., Piel, K., and Scheritz, M.: Orthomosaic Samoylov Island, Lena Delta, Siberia, <https://doi.org/10.1594/PANGAEA.786073>, 2012.
- 10 Boike, J., Kattenstroth, B., Abramova, K., Bornemann, N., Chetverova, A., Fedorova, I., Fröb, K., Grigoriev, M., Grüber, M., Kutzbach, L., Langer, M., Minke, M., Muster, S., Piel, K., Pfeiffer, E. M., Stoof, G., Westermann, S., Wischnewski, K., Wille, C., and Hubberten, H. W.: Baseline characteristics of climate, permafrost and land cover from a new permafrost observatory in the Lena River Delta, Siberia (1998–2011), *Biogeosciences*, 10, 2105–2128, 2013.
- Boike, J., Nitzbon, J., Anders, K., Grigoriev, M., Bolshiyarov, D., Langer, M., Lange, S., Bornemann, N., Morgenstern, A., Schreiber, P., 15 Wille, C., Chadburn, S., Gouttevin, I., and Kutzbach, L.: A 16-year record (2002–2017) of permafrost, active layer, and meteorological conditions at the Samoylov Island Arctic permafrost research site, Lena River Delta, northern Siberia: an opportunity to validate remote sensing data and land surface, snow, and permafrost models, *Earth System Science Data Discussions*, 2018, 1–77, 2018.
- Bolshiyarov, D., Makarov, A., and Savelieva, L.: Lena River delta formation during the Holocene, *Biogeosciences*, 12, 579–593, 2015.
- Brown, J., Ferrians Jr, O., Heginbottom, J., and Melnikov, E.: Circum-Arctic map of permafrost and ground-ice conditions, US Geological Survey Reston, 1997.
- 20 Burba, G., Schmidt, A., Scott, R. L., Nakai, T., Kathilankal, J., Fratini, G., Hanson, C., Law, B., McDermitt, D. K., Eckles, R., et al.: Calculating CO₂ and H₂O eddy covariance fluxes from an enclosed gas analyzer using an instantaneous mixing ratio, *Global Change Biology*, 18, 385–399, 2012.
- Burba, G. G., Anderson, D. J., Xu, L., and McDermitt, D. K.: Correcting apparent off-season CO₂ uptake due to surface heating of an open path gas analyzer: progress report of an ongoing study, in: *Proceedings of 27th Annual Conference of Agricultural and Forest Meteorology*, San Diego, California, 13pp, 2006.
- Burba, G. G., McDermitt, D. K., Grelle, A., Anderson, D. J., and Xu, L.: Addressing the influence of instrument surface heat exchange on the measurements of CO₂ flux from open-path gas analyzers, *Global Change Biology*, 14, 1854–1876, 2008.
- Davidson, E. A. and Janssens, I. A.: Temperature sensitivity of soil carbon decomposition and feedbacks to climate change, *Nature*, 440, 30 165, 2006.
- Ekici, A., Beer, C., Hagemann, S., and Hauck, C.: Simulating high-latitude permafrost regions by the JSBACH terrestrial ecosystem model, *Geoscientific Model Development*, 7, 631–647, 2014.
- Falge, E., Baldocchi, D., Olson, R., Anthoni, P., Aubinet, M., Bernhofer, C., Burba, G., Ceulemans, R., Clement, R., Dolman, H., Granier, A., Gross, P., Grünwald, T., Hollinger, D., Jensen, N.-O., Katul, G., Keronen, P., Kowalski, A., Lai, C. T., Law, B. E., Meyers, T., Moncrieff, J., Moors, E., Munger, J., Pilegaard, K., Rannik, Ü., Rebmann, C., Suyker, A., Tenhunen, J., Tu, K., Verma, S., Vesala, T., Wilson, K., and Wofsy, S.: Gap filling strategies for defensible annual sums of net ecosystem exchange, *Agricultural and Forest Meteorology*, 107, 43 – 35 69, 2001.



- Fan, S.-M., Wofsy, S. C., Bakwin, P. S., Jacob, D. J., and Fitzjarrald, D. R.: Atmosphere-biosphere exchange of CO₂ and O₃ in the central Amazon forest, *Journal of Geophysical Research: Atmospheres*, 95, 16 851–16 864, 1990.
- Fedorova, I., Chetverova, A., Bolshiyarov, D., Makarov, A., Boike, J., Heim, B., Morgenstern, A., Overduin, P. P., Wegner, C., Kashina, V., Eulenburg, A., Dobrotina, E., and Sidorina, I.: Lena Delta hydrology and geochemistry: long-term hydrological data and recent field observations, *Biogeosciences*, 12, 345–363, 2015.
- Finkelstein, P. L. and Sims, P. F.: Sampling error in eddy correlation flux measurements, *Journal of Geophysical Research*, 106, 3503, 2001.
- Gash, J. H. C. and Culf, a. D.: Applying a linear detrend to eddy correlation data in realtime, *Boundary-Layer Meteorology*, 79, 301 – 306, 1996.
- Grigoriev, M.: *Kriomorfogenez ust'evoy oblasti r. Leny* (Cryomorphogenesis in the Lena Delta (in Russian)), Permafrost Institute Press, Yakutsk, 1993.
- Helbig, M., Boike, J., Langer, M., Schreiber, P., Runkle, B., and Kutzbach, L.: Spatial and seasonal variability of polygonal tundra water balance: Lena River Delta, northern Siberia (Russia), *Hydrogeology Journal*, 21, 133–147, 2013.
- Holl, D. and Kutzbach, L.: A long-term (2002 to 2017) record of closed-path and open-path eddy covariance CO₂ net ecosystem exchange fluxes from the Siberian Arctic, <https://doi.pangaea.de/10.1594/PANGAEA.892751>, 2018.
- Horst, T. and Weil, J.: Footprint estimation for scalar flux measurements in the atmospheric surface layer, *Boundary-Layer Meteorology*, 59, 279–296, 1992.
- Horst, T. W. and Lenschow, D. H.: Attenuation of scalar fluxes measured with spatially-displaced sensors, *Boundary-Layer Meteorology*, 130, 275 – 300, 2009.
- Huang, C.: A theory of dispersion in turbulent shear flow, *Atmospheric Environment* (1967), 13, 453–463, 1979.
- Ibrom, A., Dellwik, E., Flyvbjerg, H., Jensen, N. O., and Pilegaard, K.: Strong low-pass filtering effects on water vapour flux measurements with closed-path eddy correlation systems, *Agricultural and Forest Meteorology*, 147, 140 – 156, 2007a.
- Ibrom, A., Dellwik, E., Larsen, S. E., and Pilegaard, K.: On the use of the Webb–Pearman–Leuning theory for closed path eddy correlation measurements, *Tellus B*, 59, 937–946, 2007b.
- IUSS Working Group WRB: World Reference Base for Soil Resources 2014, update 2015 International soil classification system for naming soils and creating legends for soil maps, *World Soil Resources Reports No. 106*, p. 192, 2015.
- Järvi, L., Mammarella, I., Eugster, W., Ibrom, A., Siivola, E., Dellwik, E., Keronen, P., Burba, G., and Vesala, T.: Comparison of net CO₂ fluxes measured with open-and closed-path infrared gas analyzers in an urban complex environment., *Boreal Environment Research*, 14, 2009.
- Kaimal, J. and Finnigan, J.: *Atmospheric Boundary Layer Flows: Their structure and measurements*, Oxford University Press, Oxford, 1994.
- Kaiser, S., Göckede, M., Castro-Morales, K., Knoblauch, C., Ekici, A., Kleinen, T., Zubrzycki, S., Sachs, T., Wille, C., and Beer, C.: Process-based modelling of the methane balance in periglacial landscapes (JSBACH-methane), *Geoscientific Model Development*, 10, 333–358, 2017.
- Khvorostyanov, D., Krinner, G., Ciais, P., Heimann, M., and Zimov, S.: Vulnerability of permafrost carbon to global warming. Part I: model description and role of heat generated by organic matter decomposition, *Tellus B*, 60, 250–264, 2008.
- Kittler, F., Eugster, W., Foken, T., Heimann, M., Kolle, O., and Göckede, M.: High-quality eddy covariance CO₂ budgets under cold climate conditions, *Journal of Geophysical Research: Biogeosciences*, 122, 2064–2084, 2017.
- Knoblauch, C., Zimmermann, U., Blumenberg, M., Michaelis, W., and Pfeiffer, E.-M.: Methane turnover and temperature response of methane-oxidizing bacteria in permafrost-affected soils of northeast Siberia, *Soil Biology and Biochemistry*, 40, 3004–3013, 2008.



- Knoblauch, C., Spott, O., Eygrafova, S., Kutzbach, L., and Pfeiffer, E.-M.: Regulation of methane production, oxidation, and emission by vascular plants and bryophytes in ponds of the northeast Siberian polygonal tundra, *Journal of Geophysical Research: Biogeosciences*, 120, 2525–2541, 2015.
- Knoblauch, C., Beer, C., Liebner, S., Grigoriev, M. N., and Pfeiffer, E.-M.: Methane production as key to the greenhouse gas budget of thawing permafrost, *Nature Climate Change*, 8, 309, 2018.
- Kormann, R. and Meixner, F. X.: An analytical footprint model for non-neutral stratification, *Boundary-Layer Meteorology*, 99, 207 – 224, 2001.
- Koven, C. D., Ringeval, B., Friedlingstein, P., Ciais, P., Cadule, P., Khvorostyanov, D., Krinner, G., and Tarnocai, C.: Permafrost carbon-climate feedbacks accelerate global warming, *Proceedings of the National Academy of Sciences*, 108, 14 769–14 774, 2011.
- 10 Kutzbach, L.: The exchange of energy, water and carbon dioxide between wet arctic tundra and the atmosphere at the Lena River Delta, Northern Siberia, *Berichte zur Polar-und Meeresforschung (Reports on Polar and Marine Research)*, 541, 2006.
- Kutzbach, L., Wagner, D., and Pfeiffer, E.-M.: Effect of microrelief and vegetation on methane emission from wet polygonal tundra, Lena Delta, Northern Siberia, *Biogeochemistry*, 69, 341–362, 2004.
- Kutzbach, L., Wille, C., and Pfeiffer, E. M.: The exchange of carbon dioxide between wet arctic tundra and the atmosphere at the Lena River Delta, Northern Siberia, *Biogeosciences*, 4, 869–890, 2007.
- 15 Kutzbach, L., Sachs, T., Boike, J., Wille, C., Schreiber, P., Langer, M., and Pfeiffer, E.-M.: FLUXNET2015 RU-Sam Samoylov, Tech. rep., FluxNet; University of Hamburg; Alfred Wegener Institute; GFZ German Research Centre for Geosciences, <https://doi.org/10.18140/FLX/1440185>, 2015.
- Langer, M., Westermann, S., Muster, S., Piel, K., and Boike, J.: The surface energy balance of a polygonal tundra site in northern Siberia Part 1: Spring to fall, *The Cryosphere*, 5, 151, 2011a.
- 20 Langer, M., Westermann, S., Muster, S., Piel, K., and Boike, J.: The surface energy balance of a polygonal tundra site in northern Siberia Part 2: Winter, *Cryosphere*, 5, 509–524, 2011b.
- Liebner, S. and Wagner, D.: Abundance, distribution and potential activity of methane oxidizing bacteria in permafrost soils from the Lena Delta, Siberia, *Environmental microbiology*, 9, 107–117, 2007.
- 25 Liebner, S., Zeyer, J., Wagner, D., Schubert, C., Pfeiffer, E.-M., and Knoblauch, C.: Methane oxidation associated with submerged brown mosses reduces methane emissions from Siberian polygonal tundra, *Journal of Ecology*, 99, 914–922, 2011.
- MacDougall, A. H., Avis, C. A., and Weaver, A. J.: Significant contribution to climate warming from the permafrost carbon feedback, *Nature Geoscience*, 5, 719, 2012.
- Mauder, M. and Foken, T.: Documentation and instruction manual of the eddy covariance software package TK2, Univ, Arbeitsergebnisse, 30 Universität Bayreuth, Abt. Mikrometeorologie, 26, 45, 2004.
- McGuire, A. D., Christensen, T. R., Hayes, D., Heroult, A., Euskirchen, E., Kimball, J. S., Koven, C., Lafleur, P., Miller, P. A., Oechel, W., Peylin, P., Williams, M., and Yi, Y.: An assessment of the carbon balance of Arctic tundra: comparisons among observations, process models, and atmospheric inversions, *Biogeosciences*, 9, 3185–3204, 2012.
- McGuire, A. D., Lawrence, D. M., Koven, C., Clein, J. S., Burke, E., Chen, G., Jafarov, E., MacDougall, A. H., Marchenko, S., Nicolsky, D., 35 et al.: Dependence of the evolution of carbon dynamics in the northern permafrost region on the trajectory of climate change, *Proceedings of the National Academy of Sciences*, p. 201719903, 2018.



- Moffat, A. M., Papale, D., Reichstein, M., Hollinger, D. Y., Richardson, A. D., Barr, A. G., Beckstein, C., Braswell, B. H., Churkina, G., Desai, A. R., Falge, E., Gove, J. H., Heimann, M., Hui, D., Jarvis, A. J., Kattge, J., Noormets, A., and Stauch, V. J.: Comprehensive comparison of gap-filling techniques for eddy covariance net carbon fluxes, *Agricultural and Forest Meteorology*, 147, 209 – 232, 2007.
- Moncrieff, J., Valentini, R., Greco, S., Guenther, S., and Ciccioli, P.: Trace gas exchange over terrestrial ecosystems: methods and perspectives in micrometeorology, *Journal of Experimental Botany*, 48, 1133 – 1142, 1997.
- Moncrieff, J., Clement, R., Finnigan, J., and Meyers, T.: Averaging, detrending, and filtering of eddy covariance time series, in: *Handbook of micrometeorology*, edited by Lee, X., Massman, W., and Law, B., pp. 7–31, Springer Netherlands, Dordrecht, 2004.
- Munger, J. W., Loescher, H. W., and Luo, H.: Measurement, tower, and site design considerations, in: *Eddy Covariance: A Practical Guide to Measurement and Data Analysis*, pp. 21–58, Springer, 2012.
- 10 Muster, S., Langer, M., Heim, B., Westermann, S., and Boike, J.: Subpixel heterogeneity of ice-wedge polygonal tundra: a multi-scale analysis of land cover and evapotranspiration in the Lena River Delta, Siberia, *Tellus B: Chemical and Physical Meteorology*, 64, 17 301, 2012.
- Nakai, T., Van der Molen, M., Gash, J., and Kodama, Y.: Correction of sonic anemometer angle of attack errors, *Agricultural and Forest Meteorology*, 136, 19–30, 2006.
- 15 Oechel, W. C., Laskowski, C. A., Burba, G., Gioli, B., and Kalhori, A. A. M.: Annual patterns and budget of CO₂ flux in an Arctic tussock tundra ecosystem, *Journal of Geophysical Research: Biogeosciences*, 119, 323–339, 2014.
- Park, T., Ganguly, S., Tømmervik, H., Euskirchen, E. S., Høgda, K.-A., Karlsen, S. R., Brovkin, V., Nemani, R. R., and Myneni, R. B.: Changes in growing season duration and productivity of northern vegetation inferred from long-term remote sensing data, *Environmental Research Letters*, 11, 084 001, 2016.
- 20 Pfeiffer, E.-M. and Grigoriev, M. N.: Russian-German Cooperation SYSTEM LAPTEV SEA 2000: The Expedition LENA 2001, Reports on Polar Research, 2002.
- Reichstein, M., Falge, E., Baldocchi, D., Papale, D., Aubinet, M., Berbigier, P., Bernhofer, C., Buchmann, N., Gilmanov, T., Granier, A., Grunwald, T., Havrankova, K., Ilvesniemi, H., Janous, D., Knohl, A., Laurila, T., Lohila, A., Loustau, D., Matteucci, G., Meyers, T., Miglietta, F., Ourcival, J.-M., Pumpanen, J., Rambal, S., Rotenberg, E., Sanz, M., Tenhunen, J., Seufert, G., Vaccari, F., Vesala, T., Yakir, D., and Valentini, R.: On the separation of net ecosystem exchange into assimilation and ecosystem respiration: review and improved algorithm, *Global Change Biology*, 11, 1424 – 1439, 2005.
- 25 Rogiers, N., Conen, F., Furger, M., Stöckli, R., and Eugster, W.: Impact of past and present land-management on the C-balance of a grassland in the Swiss Alps, *Global Change Biology*, 14, 2613–2625, 2008.
- Romanovskii, N., Hubberten, H.-W., Gavrilov, A., Tumskey, V., and Kholodov, A.: Permafrost of the east Siberian Arctic shelf and coastal lowlands, *Quaternary Science Reviews*, 23, 1359–1369, 2004.
- 30 Romanovsky, V. E., Smith, S. L., and Christiansen, H. H.: Permafrost thermal state in the polar Northern Hemisphere during the international polar year 2007–2009: a synthesis, *Permafrost and Periglacial processes*, 21, 106–116, 2010.
- Runkle, B., Sachs, T., Wille, C., Pfeiffer, E.-M., and Kutzbach, L.: Bulk partitioning the growing season net ecosystem exchange of CO₂ in Siberian tundra reveals the seasonality of its carbon sequestration strength, *Biogeosciences*, 10, 1337–1349, 2013.
- 35 Runkle, B. R., Wille, C., Gažovič, M., and Kutzbach, L.: Attenuation correction procedures for water vapour fluxes from closed-path eddy-covariance systems, *Boundary-layer meteorology*, 142, 401–423, 2012.
- Sachs, T., Wille, C., Boike, J., and Kutzbach, L.: Environmental controls on ecosystem-scale CH₄ emission from polygonal tundra in the Lena River Delta, Siberia, *Journal of Geophysical Research: Biogeosciences*, 113, 2008.



- Sachs, T., Giebels, M., Boike, J., and Kutzbach, L.: Environmental controls on CH₄ emission from polygonal tundra on the microsite scale in the Lena river delta, Siberia, *Global Change Biology*, 16, 3096–3110, 2010.
- Schneider, J., Grosse, G., and Wagner, D.: Land cover classification of tundra environments in the Arctic Lena Delta based on Landsat 7 ETM+ data and its application for upscaling of methane emissions, *Remote Sensing of Environment*, 113, 380–391, 2009.
- 5 Schneider von Deimling, T., Meinshausen, M., Levermann, A., Huber, V., Frieler, K., Lawrence, D., and Brovkin, V.: Estimating the near-surface permafrost-carbon feedback on global warming, *Biogeosciences*, 9, 649, 2012.
- Schuur, E., Abbott, B., Bowden, W., Brovkin, V., Camill, P., Canadell, J., Chanton, J., Chapin, F., Christensen, T., Ciais, P., et al.: Expert assessment of vulnerability of permafrost carbon to climate change, *Climatic Change*, 119, 359–374, 2013.
- Schuur, E., McGuire, A. D., Schädel, C., Grosse, G., Harden, J., Hayes, D., Hugelius, G., Koven, C., Kuhry, P., Lawrence, D., et al.: Climate
10 change and the permafrost carbon feedback, *Nature*, 520, 171–179, 2015.
- Schuur, E. A., Bockheim, J., Canadell, J. G., Euskirchen, E., Field, C. B., Goryachkin, S. V., Hagemann, S., Kuhry, P., Lafleur, P. M., Lee, H., et al.: Vulnerability of permafrost carbon to climate change: Implications for the global carbon cycle, *AIBS Bulletin*, 58, 701–714, 2008.
- Schwamborn, G., Rachold, V., and Grigoriev, M. N.: Late Quaternary sedimentation history of the Lena Delta, *Quaternary international*, 89, 119–134, 2002.
- 15 Soil Survey Staff: *Keys to Soil Taxonomy*, Twelfth Edition, 2014.
- Tarnocai, C., Canadell, J., Schuur, E., Kuhry, P., Mazhitova, G., and Zimov, S.: Soil organic carbon pools in the northern circumpolar permafrost region, *Global biogeochemical cycles*, 23, 2009.
- Van Ulden, A.: Simple estimates for vertical diffusion from sources near the ground, *Atmospheric Environment (1967)*, 12, 2125–2129, 1978.
- 20 Vickers, D. and Mahrt, L.: Quality control and flux sampling problems for tower and aircraft data, *Journal of Atmospheric and Oceanic Technology*, 14, 512 – 526, 1997.
- Wagner, D., Kobabe, S., Pfeiffer, E.-M., and Hubberten, H.-W.: Microbial controls on methane fluxes from a polygonal tundra of the Lena Delta, Siberia, *Permafrost and periglacial processes*, 14, 173–185, 2003.
- Walker, H. J.: Arctic deltas, *Journal of Coastal Research*, pp. 719–738, 1998.
- 25 Wania, R., Ross, I., and Prentice, I.: Integrating peatlands and permafrost into a dynamic global vegetation model: 2. Evaluation and sensitivity of vegetation and carbon cycle processes, *Global Biogeochemical Cycles*, 23, 2009a.
- Wania, R., Ross, I., and Prentice, I. C.: Integrating peatlands and permafrost into a dynamic global vegetation model: 1. Evaluation and sensitivity of physical land surface processes, *Global Biogeochemical Cycles*, 23, 2009b.
- Wania, R., Ross, I., and Prentice, I.: Implementation and evaluation of a new methane model within a dynamic global vegetation model:
30 LPJ-WHyMe v1. 3.1, *Geoscientific Model Development*, 3, 565, 2010.
- Webb, E. K., Pearman, G. I., and Leuning, R.: Correction of flux measurements for density effects due to heat and water vapour transfer, *Quarterly Journal of the Royal Meteorological Society*, 106, 85–100, 1980.
- Wille, C., Kutzbach, L., Sachs, T., Wagner, D., and PFEIFFER, E.-M.: Methane emission from Siberian arctic polygonal tundra: eddy covariance measurements and modeling, *Global Change Biology*, 14, 1395–1408, 2008.
- 35 Wutzler, T., Moffat, A., Migliavacca, M., Knauer, J., Menzer, O., Sickel, K., and Reichstein, M.: Reddyproc: Enabling researchers to process eddy-covariance data, in: *EGU General Assembly Conference Abstracts*, vol. 19, p. 12954, 2017.
- Yershov, E. D.: *General geocryology*, Cambridge University Press, 2004.
- Zimov, S. A., Schuur, E. A., and Chapin, F. S.: Permafrost and the global carbon budget, *Science*, 312, 1612–1613, 2006.



Zona, D., X., X., Hufkens, K., Gioli, B., Burba, G., Goodrich, J. P., Liljedahl, A. K., Euskirchen, E. S., Watts, J. D., Kimball, J. S., Heimann, M., Goeckede, M., Kittler, F., Lund, M., Dolman, H., Belelli Marchesini, L., Commane, R. S., Wofsy, C., Miller, C. E., Lipson, D. A., Kalhori, K. A., Arndt, A., Kutzbach, L., Boike, J., Wille, C., Holl, D., Sachs, T., Song, X., Humphreys, E. R., Lafleur, P. M., Koven, C. D., and Oechel, W. C.: Pan-Arctic temperature response of tundra carbon sequestration across scales, in review.

- 5 Zubrzycki, S., Kutzbach, L., Grosse, G., Desyatkin, A., and Pfeiffer, E.-M.: Organic carbon and total nitrogen stocks in soils of the Lena River Delta, *Biogeosciences*, 10, 3507, 2013.

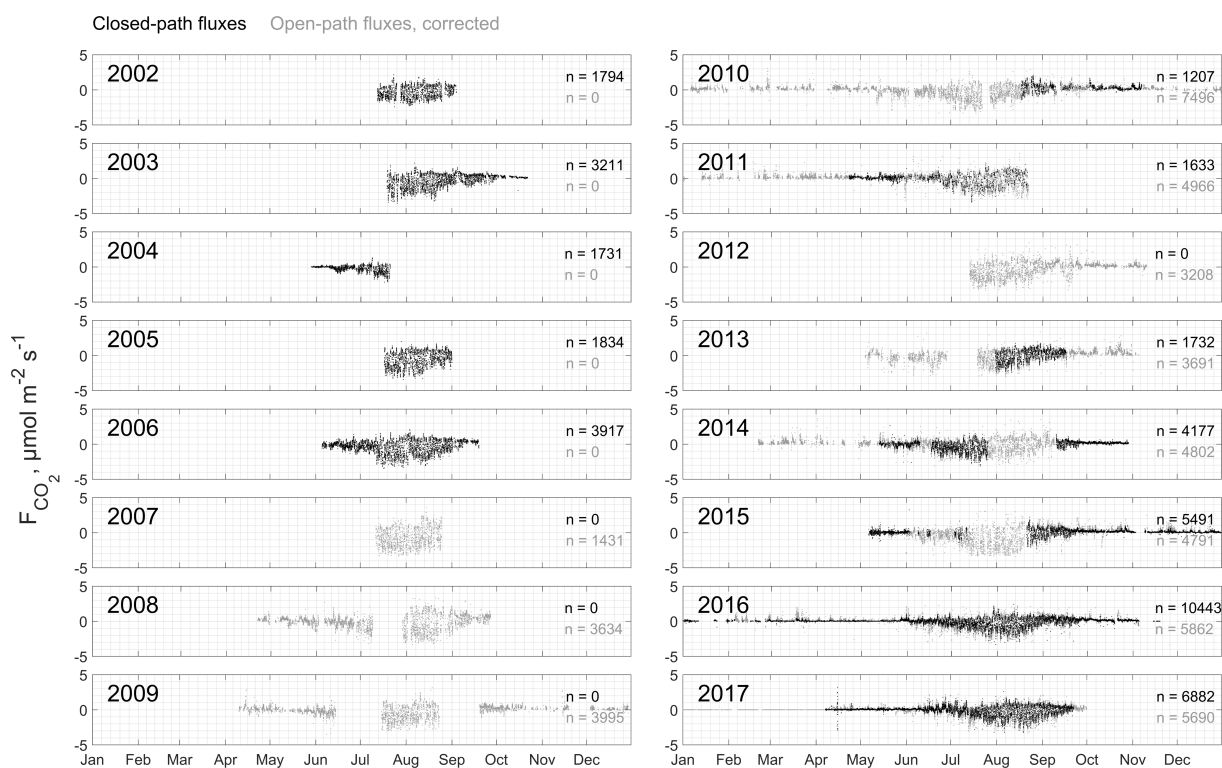


Figure 3. Multiannual time series of the presented closed-path (black dots) and open-path (gray dots) flux datasets from Samoylov Island's river terrace. Fluxes of quality class 2 are not shown. Self-heating errors in the OP dataset have been corrected for.

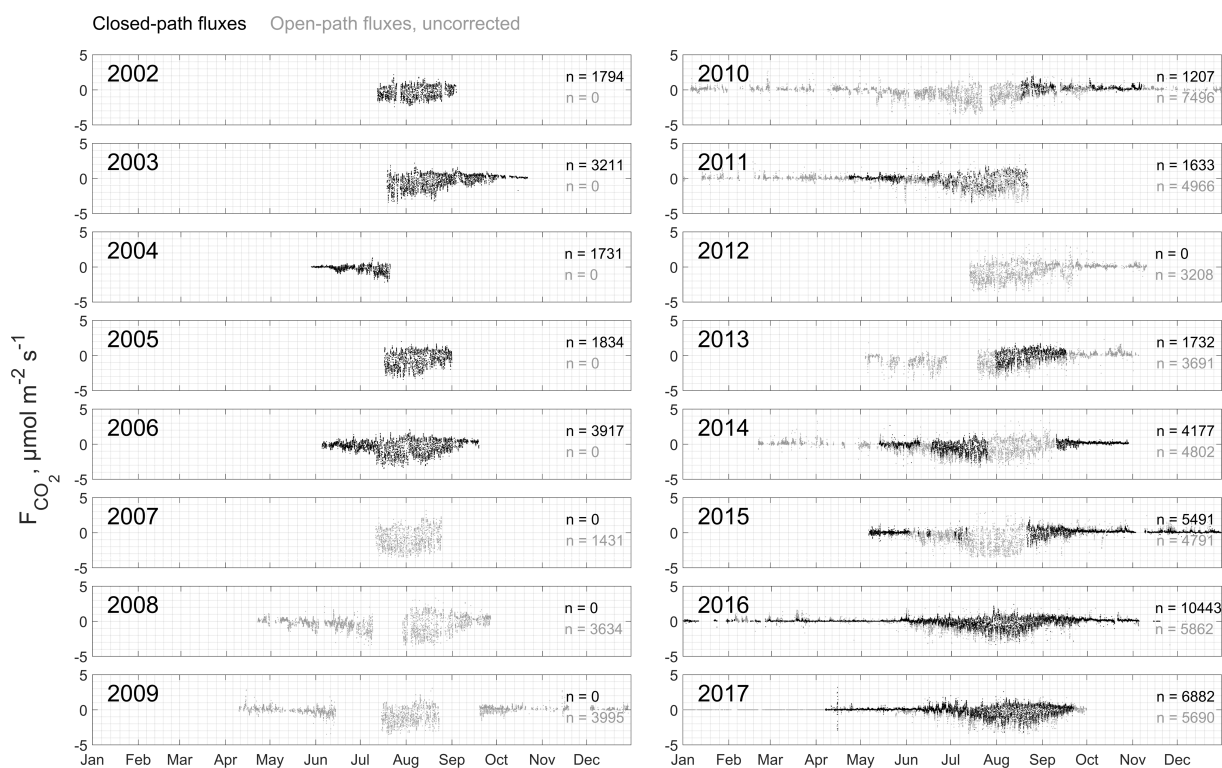


Figure 4. Multiannual time series of the presented closed-path (black dots) and uncorrected open-path (gray dots) flux datasets from Samoylov Island's river terrace. Fluxes of quality class 2 are not shown.



Table 1. List of deployed instrument types. All infrared gas analyzers were manufactured by LI-COR Biosciences (USA), R3 sonic anemometers were built by Gill Instruments Ltd. (UK), CSAT3 anemometers by Campbell Scientific Ltd. (UK)

Year	Gas analyzer		Anemometer		Data coverage	
	Closed path	Open path	Model	Height, m	Date range	Days
2002	LI-7000	n/a	R3	3.65	12-Jul to 03-Sep	53
2003	LI-7000	n/a	R3	3.65	19-Jul to 22-Oct	95
2004	LI-7000	n/a	R3	3.65	28-May to 20-Jul	53
2005	LI-7000	n/a	R3	4	17-Jul to 01-Sep	46
2006	LI-7000	n/a	R3	4	05-Jun to 19-Sep	106
2007	n/a	LI-7500	CSAT3	2.4	11-Jul to 23-Aug	36
2008	n/a	LI-7500	CSAT3	2.4	22-Apr to 26-Sep	157
2009 I	n/a	LI-7500	CSAT3	2.4	10-Apr to 14-Jun	65
2009 II	n/a	LI-7500	CSAT3	4.15	15-Jul to 29-Dec	167
2010	LI-7000	LI-7500	CSAT3	4.15	01-Jan to 31-Dec	359
2011	LI-7000	LI-7500	CSAT3	4.15	01-Jan to 22-Aug	233
2012	n/a	LI-7500	CSAT3	4.15	13-Jul to 10-Nov	120
2013	LI-7000	LI-7500A	CSAT3	4.15	04-May to 05-Nov	185
2014	LI-7000	LI-7500A	CSAT3	4.15	21-Feb to 29-Oct	250
2015	LI-7000	LI-7500A	CSAT3	4.15	06-May to 31-Dec	239
2016	LI-7000	LI-7500A	CSAT3	4.15	01-Jan to 19-Nov	323
2017	LI-7000	LI-7500A	CSAT3	4.15	01-Jan to 30-Sep	272



Table 2. Eddy covariance flux processing steps. Partly differing processing was applied to raw data from closed and open-path analyzers. OP and CP fluxes were computed consistently for the whole period from 2002 to 2017. Setup-dependent statistics (for time lags and *in situ* spectral correction methods) were evaluated annually or if tower position, CP pump speed or any other analyzer metadata changed.

Processing step	Method	
	Closed path data	Open path data
Spike detection & removal	raw data spike removal (Vickers and Mahrt, 1997)	
Angle of attack correction	from 2002 to 2006 during Gill anemometer deployment (Nakai et al., 2006)	n/a, sensor was not deployed between 2002 and 2006
Axis rotation	Double rotation (Kaimal and Finnigan, 1994)	
Detrending	linear, (Gash and Culf, 1996)	
Correction for air density fluctuations	sample-wise conversion of raw data to mixing ratios (Ibrom et al., 2007b; Burba et al., 2012)	application of WPL-Terms to fluxes (Webb et al., 1980)
Time lag compensation	covariance maximization with nominal time lag from statistics	covariance maximization
Spectral corrections for		
High-pass filtering	analytic (Moncrieff et al., 2004)	
Low-pass filtering	<i>in situ</i> /analytic (Ibrom et al., 2007a)	analytic (Moncrieff et al., 1997)
Instrument separation	Horst and Lenschow (2009)	n/a
Eddy Pro version	≥ 6.0.0	



Table 3. Additional quality flagging steps after flux processing. Flagged fluxes were assigned to quality class 2 if not in this class already according to the Mauder and Foken (2004) quality assessment. As CP time lag detection quality had been addressed earlier during flux processing in EddyPro, it was not screened at this stage.

Step	Applied to		# of flagged fluxes	
	OP fluxes	CP fluxes	OP	CP
1: Raw data skewness/kurtosis	yes	yes	23769 (23 %)	12043 (18 %)
2: Instrument signal strength	yes	no	6951 (7 %)	n/a
3: Time lag detection quality	yes	no	20277 (20 %)	n/a
4: Absolute concentration limits	yes	yes	223 (0.2 %)	2261 (3 %)
5: Exclusion of outliers when simultaneous CP fluxes close to zero	yes	n/a	346 (0.3 %)	n/a
6: Absolute flux limits	yes	yes	634 (0.6 %)	102 (0.6 %)



Table 4. Estimates of scaling factor $\xi \pm 95\%$ confidence intervals used for open-path flux correction. ξ describes the portion of the self-heating correction term, given by Burba et al. (2006) for vertically installed instruments, that is needed to correct OP fluxes determined with inclined gas analyzers. The scaling factor was optimized as a parameter of a nonlinear function where CP data were regarded as true fluxes. It was therefore determined for years when parallel CP and OP measurements were available. In case of an optimization converging to unreasonable values (below zero), we used the median of the remaining ξ estimates.

Year	Daytime ξ	Nighttime ξ
2010	0.0076 ± 0.0012	0.0071 ± 0.0013
2011	0.0116 ± 0.0009	0.0068 ± 0.0015
2013	0.0150 ± 0.0007	0.0104 ± 0.0009
2014	0.0094 ± 0.0006	0.0071
2015	0.0050 ± 0.0010	0.0071
2016	0.0051 ± 0.0005	0.0071
2017	0.0069 ± 0.0005	0.0071



Table 5. Normalized mean contributions of the surface classes defined by Muster et al. (2012) to the eddy covariance footprint. Values were averaged over each subperiod and normalized to sum up to 1. Additionally, the mean non-normalized sum of all surface class contributions is given as column *Image contribution*. These values indicate how sufficient the classified area is to describe the EC footprint. Non-normalized half-hourly contributions of the single classes are given in the provided data set.

Year	Tundra		Water		Median image contribution
	<i>dry</i>	<i>wet</i>	<i>overgrown</i>	<i>open</i>	
2002	0.71	0.17	0.07	0.05	0.88
2003	0.70	0.17	0.07	0.05	0.87
2004	0.71	0.16	0.07	0.06	0.88
2005	0.71	0.17	0.07	0.05	0.87
2006	0.70	0.17	0.07	0.06	0.86
2007	0.54	0.37	0.06	0.02	0.73
2008	0.53	0.34	0.09	0.04	0.77
2009 I	0.54	0.32	0.08	0.06	0.72
2009 II	0.64	0.19	0.09	0.08	0.71
2010	0.65	0.18	0.09	0.08	0.73
2011	0.67	0.18	0.08	0.07	0.79
2012	0.67	0.18	0.08	0.07	0.80
2013	0.69	0.17	0.08	0.06	0.83
2014	0.66	0.18	0.08	0.07	0.77
2015	0.66	0.18	0.08	0.08	0.78
2016	0.65	0.18	0.09	0.08	0.74
2017	0.67	0.18	0.08	0.07	0.82

**Table 6.** Description of columns included in the data set file.

Column name	Unit/Format	Description
Date/Time (Local)	yyyy-mm-ddTHH:MM	Timestamp referring to end of 30 minute flux calculation period in local time (UTC+9h).
Date/Time (UTC)	yyyy-mm-ddTHH:MM	Timestamp referring to end of 30 minute flux calculation period in UTC.
CP CO ₂ flux	$\mu\text{mol m}^{-2} \text{s}^{-1}$	Closed path CO ₂ flux
QC CP CO ₂ flux	dimensionless	Closed path CO ₂ flux quality classes 0, 1 and 2
CP CO ₂ flux rand unc	$\mu\text{mol m}^{-2} \text{s}^{-1}$	Closed path CO ₂ flux random uncertainty estimate (Finkelstein and Sims, 2001)
OP CO ₂ flux	$\mu\text{mol m}^{-2} \text{s}^{-1}$	Open path CO ₂ flux
OP corr CO ₂ flux	$\mu\text{mol m}^{-2} \text{s}^{-1}$	Corrected open-path CO ₂ flux (Kittler et al., 2017)
QC OP CO ₂ flux	dimensionless	Open path CO ₂ flux quality classes 0,1 and 2
OP CO ₂ flux rand unc	$\mu\text{mol m}^{-2} \text{s}^{-1}$	Open path CO ₂ flux random uncertainty estimate (Finkelstein and Sims, 2001)
CO ₂ flux comp	$\mu\text{mol m}^{-2} \text{s}^{-1}$	Time series compiled of open and closed-path quality class 0 and 1 fluxes
CO ₂ flux gf	$\mu\text{mol m}^{-2} \text{s}^{-1}$	Gap filled CO ₂ flux time series
QC CO ₂ flux gf	dimensionless	Quality flag of gap-filled fluxes, between 0 and 3 (Reichstein et al., 2005)
CO ₂ flux gf std	$\mu\text{mol m}^{-2} \text{s}^{-1}$	Standard deviation of gap-filled flux estimates, calculated from the data used for averaging
FP CC dry	dimensionless	Contribution of surface class <i>dry tundra</i> to the eddy covariance footprint
FP CC wet	dimensionless	Contribution of surface class <i>wet tundra</i> to the eddy covariance footprint
FP CC ove	dimensionless	Contribution of surface class <i>overgrown water</i> to the eddy covariance footprint
FP CC wat	dimensionless	Contribution of surface class <i>open water</i> to the eddy covariance footprint